

Investigation on Mechanochemical Behavior of CaHPO₄-Ca(OH)₂-Al₂O₃ System to Produce Hydroxyapatite-based Composite Nanopowders

R. Ebrahimi-Kahrizsangi, B. Nasiri-Tabrizi

Advanced Materials Research Center, Materials Engineering Department, Najafabad Branch, Islamic Azad University, Isfahan, Iran
rezaebrahimi@iaun.ac.ir, bahman_nasiri@hotmail.com

Abstract - The mechanochemical behavior of CaHPO₄-Ca(OH)₂-Al₂O₃ system to synthesize hydroxyapatite-alumina (HAp-Al₂O₃) composite nanopowders was studied. For this purpose, the structural features of the samples with different amounts of α -Al₂O₃ (0, 15, 20, 30, and 40 wt%) were investigated after 60 h of milling. Results showed that the crystallinity degree of the composite was influenced strongly by the alumina content. In the absence of alumina, the crystallite size, lattice strain, volume fraction of grain boundary, and the crystallinity degree of HAp were about 24 nm, 0.00086, 11.53 % and 83 %, respectively. In accordance with the TEM images, the synthesized HAp was composed of nanorods with an average size of about 17±8 nm. In addition, the coalescence of nanoparticles caused the agglomeration. In the presence of 15–40 wt% alumina, HAp-Al₂O₃ composite nanopowders were produced after 60 h of milling. With increasing the alumina content to 40 wt%, the crystallite size and crystallinity degree declined drastically and reached a minimum around 24 nm and 16 %, respectively. According to the obtained data, the lattice parameters of HAp in the composite structures were similar to the standard values. However, the unit cell volume values fluctuated during the milling due to the lattice distortion of HAp.

Keywords: HAp-Al₂O₃, Composite nanopowder, Mechanochemical, Crystallinity degree, Nanorod.

1. Introduction

Over the past few decades, there has been a major advance in the development of bioceramics for skeletal repair and reconstruction. Bioceramics are now used in a number of various applications throughout the body. In accordance with the type of bioceramics used and their interaction with the host tissue, they can be categorized as either *bioinert* or *bioactive* and the *bioactive* ceramics may be resorbable or non-resorbable. The most well-known types of this class of materials include: polycrystalline materials; glasses, glass ceramics and ceramic-filled bioactive composites which may be used as porous or in dense form in bulk, as granules or in the form of coatings (Hensch, 1998, Best et al. 2008). Among various types of bioceramics, hydroxyapatite (HAp, Ca₁₀(PO₄)₆(OH)₂) is one of the most common ceramics for biomedical applications (Zhou et al., 2011). However, synthetic HAp (s-HAp) has some weaknesses (Chen et al., 2005, Pushpakanth et al. 2008). For example, in spite of its suitable biological responses, the mechanical properties (toughness and bending strength) of s-HAp are poor which severely hinder its clinical applications.

In recent years, the improvements of mechanical properties of s-HAp have been attempted by a number of investigations. These studies have shown that such features of HAp might be exceptionally strengthened by one-dimensional nanoscale building blocks, such as nanorods, nanotubes and nanofibers (Honarmandi et al. 2010). From the other point of view, nanocomposites have received much attention due to their superior mechanical properties in comparison to their large-grained counterparts (Viswanath et al., 2006). It has been found that the addition of appropriate amounts of reinforcements to HAp can enhance its mechanical properties. In fact, HAp-based nanocomposites are emerging as potential alternatives for bone replacement due to improved mechanical and biological properties (Kuntz et al., 2004, Ben-Nissan, 2004). According to literature, the following conditions should be satisfied to be effective as a reinforcing agent for a bionanocomposite. Firstly, the strength and the elastic modulus of the second phase must be higher than those of the matrix. Secondly, the interfacial strength between the matrix and the second phase should be neither too weak nor too strong, so that no excessive reaction occurs between the matrix and the second phase. Thirdly, the thermal expansion coefficient of the second phase should not differ too much from that of the matrix. This feature is essential in order to prevent the micro-cracks formation during the densification

process. Fourthly, the biocompatibility of the reinforcing agent should be considered (Kong et al., 1999, Ebrahimi-Kahrizangi et al., 2010) . Among various reinforcing agents, alumina is the one of the most widely investigated reinforcement materials for HAp bioceramics (Li et al., 1995, Kim et al. 2002) . This nanocomposite is attractive materials for implant applications. However, there has been very limited work on the structural evolutions of HAp–Al₂O₃ nanocomposites during the solid-state reactions (Viswanath et al., 2006) . Hence, in the present study, the mechanochemical behavior of CaHPO₄–Ca(OH)₂–Al₂O₃ system to synthesize HAp–Al₂O₃ composite nanopowders was studied. The mechanochemical synthesis as a dry method is used to produce any quantity of nanopowder with controlled microstructure. The simplicity, reproducibility, and low processing cost are the main advantages of this method (Suryanarayana, 2001, Nasiri-Tabrizi et al., 2009) . In addition, melting and precisely controlled conditions are not essential and the products have nanostructural characteristics (Silva et al., 2004) . Therefore, mechanochemical method as employed in this research can be served, when the mass production of HAp nanopowders is required.

According to our previous findings (Nasiri-Tabrizi et al., 2013a, Ebrahimi-Kahrizangi et al. 2011, Fahami et al., 2013) , the formation of apatite nanopowders like HAp, fluorapatite (FAP), and chlorapatite (CAp) was influenced effectively by the milling time, chemical composition, and subsequent annealing. Besides, the formation of apatite nanopowders usually occurred in several steps. In the present study, the possibility of mechanochemical synthesis of HAp–Al₂O₃ composite nanopowders was studied. The structural features of the composites with different amounts of α-Al₂O₃ were investigated and compared to determine the optimum composition.

2. Experimental Procedure

Fig. 1 shows a schematic view of the preparation of HAp–Al₂O₃ composite nanopowders. Calcium hydroxide (Ca(OH)₂, Fluka), anhydrous calcium hydrogen phosphate (CaHPO₄, Merck), and alumina (α-Al₂O₃, Merck) were used as the starting chemicals.

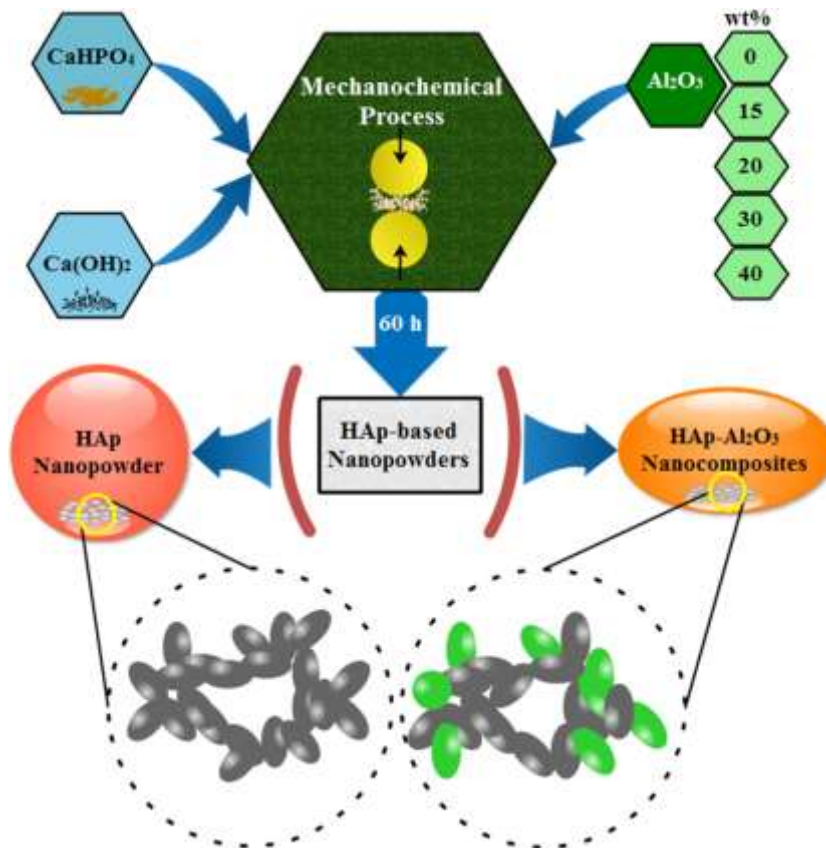
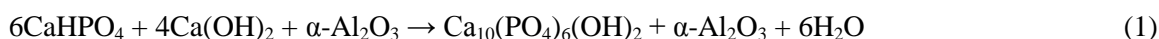


Fig. 1. A schematic view of the preparation of HAp–Al₂O₃ composite nanopowders.

The mole ratio of calcium to phosphorous was equal to 1.67. Mechanochemical synthesis was carried out in a high energy planetary ball mill at rotational speed of 600 rpm and BPR of 20:1 under ambient air atmosphere using Polyurethane vials (vol. 125 ml) and Zirconia balls (20 mm in diameter). To synthesize HAP–Al₂O₃ composite nanopowders, different amounts of alumina (0, 15, 20, 30, 40 wt %) were mixed with appropriate quantities of Ca(OH)₂ and CaHPO₄ and then the mixed powders were milled for 60 h (reaction (1)).



X-ray diffraction (Philips X-ray diffractometer (XRD)) was carried out using *Cu-K_α* radiation to evaluate the phase purity and the crystallographic structural properties of the composite nanopowders. The diffractometer was operated at 40 kV and 30 mA. "PANalytical X'Pert HighScore" software was also used to analyze the XRD data. The XRD patterns were compared to standards compiled by the Joint Committee on Powder Diffraction and Standards (JCPDS), which involved card #24-0033 for HAp, #009-0080 for CaHPO₄, and #010-0173 for α-Al₂O₃. The size and morphology of HAp nanopowder were observed on a transmission electron microscope (TEM, ZEISS, Germany) that operated at the acceleration voltage of 80 kV.

3. Results and Discussion

3.1. Mechanochemical Synthesis of HAP–Al₂O₃ Composite

Fig. 2 shows the XRD profile of the mechanochemical synthesized powder in the absence of alumina. According to this figure, milling for 60 h in the absence of Al₂O₃ resulted in the formation of a HAp nanopowder. Besides, additional peaks belonging to CaHPO₄ were detected which could be a trace of the original product of the original reaction used to produce HAp nanopowder. Similarly, CaHPO₄ as an additional phase was identified in previous investigations (Nasiri-Tabrizi et al., 2009, Silva et al., 2004).

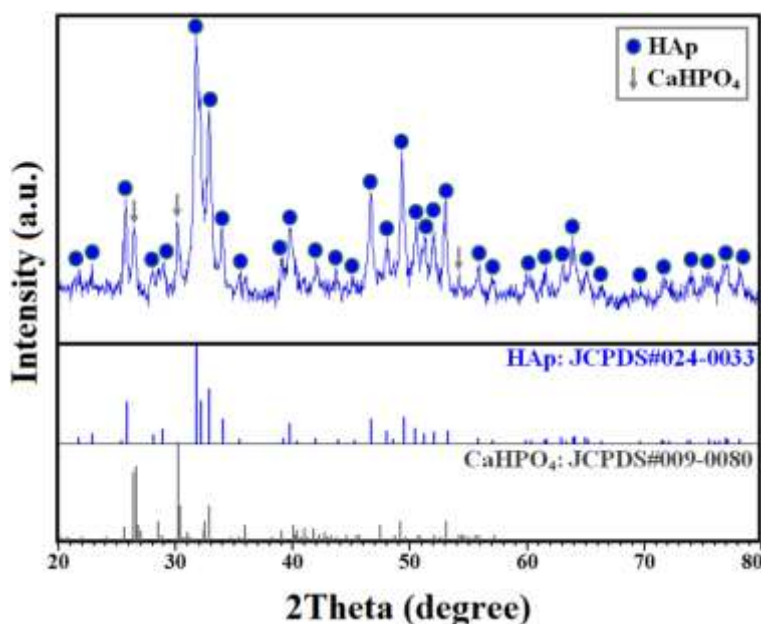


Fig. 2. XRD profile of the mechanochemical synthesized HAp powder in the absence of alumina.

The TEM image of the synthesized powder is shown in Fig. 3. From TEM image, the obtained powder had high tendency to agglomerate due to the coalescence of fine particles. However, it is obvious that each agglomerate was composed of nanorods with a mean size of about 17±8 nm. When two adjacent primary particles collide, the coalescence may take place on the premise that these two particles share a common crystallographic orientation. So, two primary particles attach to each other and combine into a secondary one. Since the sizes of the secondary particles are still very small, it is reasonable that they will continue to collide and coalesce which may ultimately lead to the agglomeration (Zhang et al., 2006). It has been found that the bioceramic nanopowders with ellipse-

or rod-like morphology inhibit the proliferation of malignant melanoma cells and may be helpful to remedy cancer (Li et al., 2008) . Therefore, the synthesized powder can be considered in biomedical applications.

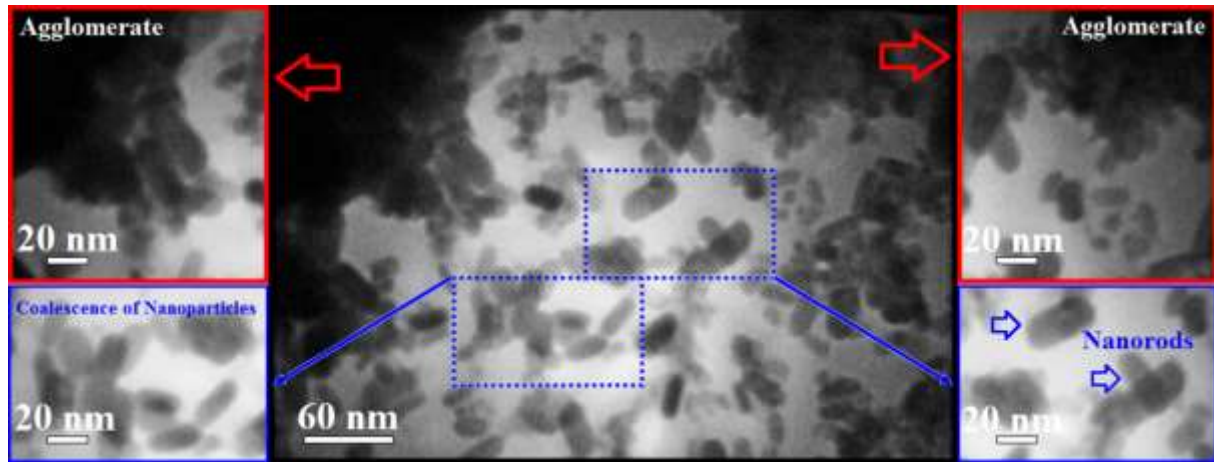


Fig. 3. TEM image of the mechano-synthesized HAp powder in the absence of alumina.

Fig. 4 displays the XRD patterns of the milled samples with different amounts of alumina after 60 h of milling. In all the specimens, mechanical activation led to the formation of HAp–Al₂O₃ composite nanopowder. In the presence of 15 wt% alumina, a HAp–15 wt% Al₂O₃ composite nanopowder was produced after 60 h of milling. Besides, similar to the previous sample, additional peaks corresponding to CaHPO₄ were observed. With increasing the alumina content to 40 wt%, a composite nanopowder (HAp–40 wt% Al₂O₃) was formed after 60 h of milling. Of course, it is evident that with increasing the alumina content the characteristic peaks of additional phase (CaHPO₄) decreased and reached a minimum in the presence of 40 wt% Al₂O₃. In addition, it can be seen that increasing the alumina content from 15 to 40 wt% caused a decrease in the fraction of crystalline phase, as evidenced by the extra broadening of the characteristic diffraction peaks. The influence of alumina content on the phase compositions of the nanocomposite are shown in Fig. 5. According to the schematic views, HAp was the main component of the 60 h milled sample in the absence of alumina. However, CaHPO₄ was present as an additional phase. In the presence of 15 wt% Al₂O₃, the phase compositions were HAp and Al₂O₃ as a result of the formation of the HAp–15 wt% Al₂O₃ composite. With increasing the alumina content to 40 wt%, no change in the phase components was found. However, the volume fraction of phases was changed owing to the increasing amount of alumina.

3.2. Crystallite Size, Lattice Strain, and Volume Fraction of Grain Boundary

The crystallite size and lattice strain of the samples were determined using the following method (Suryanarayana, 2001):

$$B \cos \theta = \frac{0.9\lambda}{D} + \eta \sin \theta . \quad (2)$$

where λ , D , η and θ are the wavelength of the X–ray used (0.154056 nm), crystallite size, internal micro-strain and the Bragg angle ($^{\circ}$), respectively. Note that B in the above equation is the peak width (in radians) after subtracting the peak width due to instrumental broadening from the experimentally recorded profile. Therefore, when $B \cos \theta$ was plotted against $\sin \theta$, straight lines were obtained for samples with the slope as η and the intercept as $0.9 \lambda / D$.

In addition, if we assume that a crystallite is a sphere of diameter D surrounded by a shell of grain boundary with thickness t , the volume fraction of grain boundary (f) is approximately (Sun et al., 2002):

$$f = 1 - \left[\frac{D}{(D+t)} \right]^3 \quad (3)$$

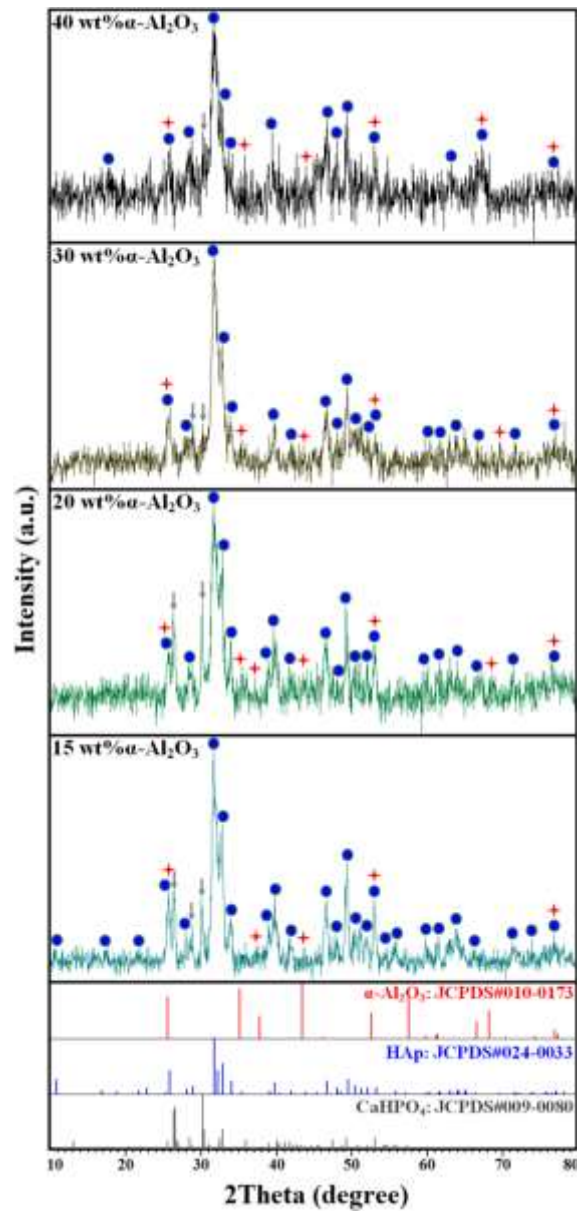


Fig. 4. XRD patterns of the milled samples with different amounts of alumina after 60 h of milling.

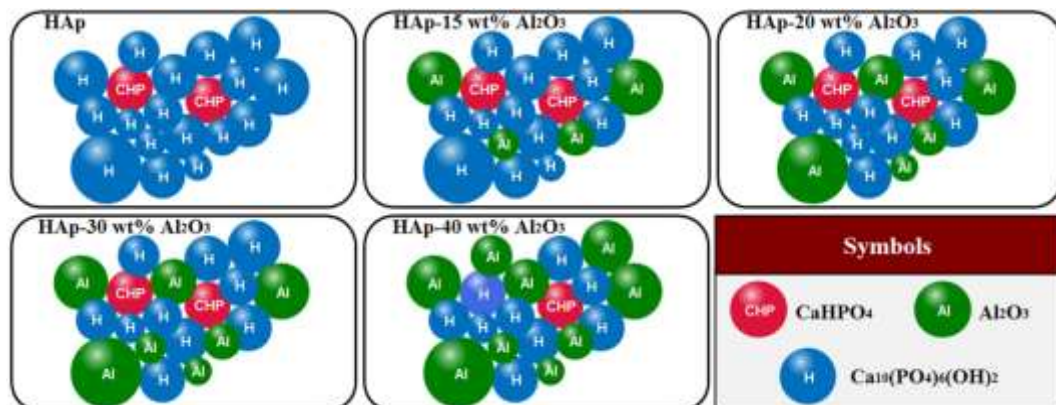


Fig. 5. The influence of alumina content on the phase compositions of the nanocomposite.

Fig. 6 shows the crystallite size, lattice strain, and volume fraction of grain boundary of the milled samples with different amounts of alumina after 60 h of milling. In the absence of alumina, the crystallite size, lattice strain, and volume fraction of grain boundary of HAp were about 24 nm, 0.00086, and 11.53 %, respectively. With the addition of 15 wt% alumina, the crystallite size increased to 34 nm, while the lattice strain decreased to 0.00085. Moreover, the volume fraction of grain boundary reached around 8.33 %. It is quite clear that with increasing the alumina content from 15 to 40 wt%, the crystallite size declined drastically to about 24 nm. In contrast, the lattice strain and volume fraction of grain boundary increased significantly to 0.00132 and 11.53 %, respectively. Owing to the mechanical deformation introduced into the powder, the number of crystal defects like dislocations, vacancies, grain boundaries and so on increased with alumina content and these provided short-circuit diffusion paths. In these circumstances, particle and crystallite refinement happened and the lattice strain increased. This result is in good agreement with previous studies (Ebrahimi-Kahrizsangi et al., 2010, Nasiri-Tabrizi et al., 2013b) . According to the obtained data, it can be concluded that the structural features of the mechanosynthesized HAp–Al₂O₃ composite nanopowders were strongly influenced by the alumina content.

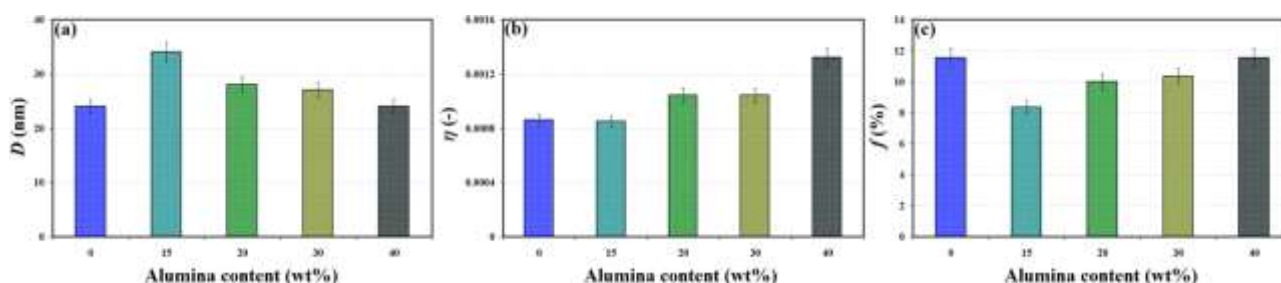


Fig. 6. Crystallite size, lattice strain, and volume fraction of grain boundary of the milled samples as a function of alumina content.

3.3. Crystallinity Degree (X_c)

The crystallinity degree (X_c) in terms of the fraction of crystalline phase present in the examined volume was estimated by taking the sum total of relative intensities of individual characteristic peaks according to the following equation (Nasiri-Tabrizi et al., 2014):

$$X_C = \frac{\text{Sum } (I_1 : I_n)_{\text{HAp}}}{\text{Sum } (I_1 : I_n)_{\text{Standard}}} \times 100 \quad (4)$$

where I₁:I_n is the total of relative intensities of characteristic peaks of HAp for both the synthesized powders and standard.

Fig. 7 shows the crystallinity degree of the synthesized nanopowders in the absence and presence of different amounts of alumina after 60 h of milling. According to this figure, the crystallinity degree of the HAp nanopowder was around 83 % in the absence of alumina. With the addition of 15 wt% alumina, the crystallinity degree decreased noticeably to around 49 %. In the presence of 20 wt% alumina, the fraction of crystalline phase was further reduced to 47 %. Further increasing the alumina content to 30 wt% was associated with greater reduction of crystallinity degree (35 %). Finally, in the presence of 40 wt% alumina, the crystallinity degree reached a minimum around 16 %. It has been reported that apatites with high crystallinity degree display little or no activity towards bioresorption and are insoluble in physiological environment (Seckler et al., 1999) . Therefore, the obtained HAp powder in the absence of alumina are well preferred for dental applications. On the other hand, apatites with low crystallinity degree show high osteoconductivity (Sonash et al., 2009) . Accordingly, the synthesized HAp–Al₂O₃ composite nanopowders especially in the presence of 40 wt% alumina can be used to promote osseointegration or as a coating to promote bone ingrowth in to prosthetic implants. These results suggest that the crystallinity degree of the mechanosynthesized HAp bioceramics was effectively influenced by the alumina content.

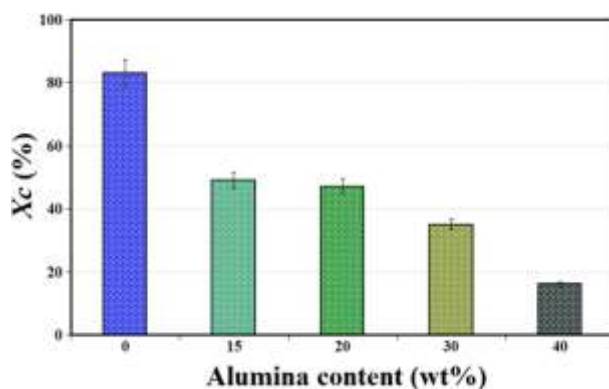


Fig. 7. Crystallinity degree of the synthesized nanopowders as a function of alumina content.

3.4. Lattice Parameters

Unit cell measurements (a -axis, c -axis, and unit cell volume (V)) of HAp as a function of alumina content are shown in Fig. 8. In accordance with Fig. 8a, the a -axis and c -axis values of HAp in the absence and presence of different amounts of alumina were similar to the reported values for standard (#24-0033: $a = 9.432 \text{ \AA}$ and $c = 6.881 \text{ \AA}$). As shown in Fig. 8b, the unit cell volume of HAp fluctuated during the milling process. The obtained data showed that the maximum and minimum values of the unit cell volume belonged to the samples with 15 and 30 wt% alumina, respectively. These variations in unit cell volume resulted mainly from a rise in the (c) parameter, rather than from the (a) values and is presumably due to the lattice distortion of HAp during the mechanochemical process. This result is in good agreement with the previous studies (Fathi et al., 2009). So it can be concluded that the values of unit cell parameters of HAp were influenced by the alumina content.

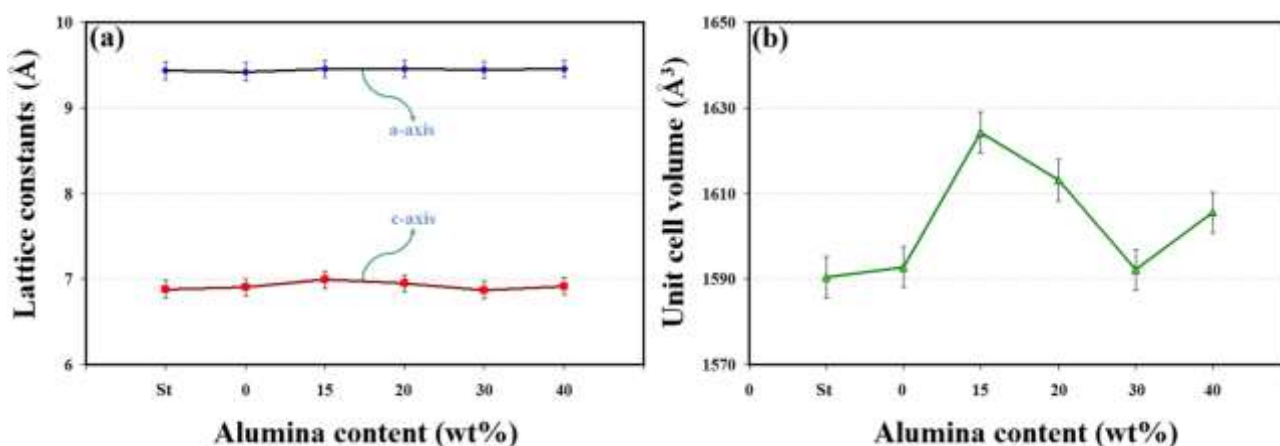


Fig. 8 Unit cell measurements of HAp as a function of alumina content. (a) a -axis, c -axis, and (b) unit cell volume values.

3.5. Reaction Mechanism

Fig. 9 shows the reaction mechanism of the formation of HAp- Al_2O_3 composite nanopowders during the mechanochemical synthesis. According to this figure and the obtained results, the following reaction mechanism have been proposed to clarify the reactions occurring during the milling. As a matter of fact, various mechanochemical reactions may happen under the milling process. In these reactions, the raw materials consumption rate may vary depending on the stoichiometric proportionality between the materials and the milling circumstances. In this work, the formation of HAp- Al_2O_3 composite nanopowder was strongly influenced by the alumina content. As previously mentioned, CaHPO_4 , $\text{Ca}(\text{OH})_2$, and $\alpha\text{-Al}_2\text{O}_3$ were employed as the raw materials. According to the XRD profiles, in the absence of alumina the reaction of CaHPO_4 with $\text{Ca}(\text{OH})_2$ resulted in the formation of high crystalline HAp nanopowder. With the addition of various amounts of alumina, no interfacial reaction occurred between the calcium phosphate reagents and alumina. In fact, in all the sample, the main product of milling for 60 h was HAp- Al_2O_3 composite nanopowder. However, the volume fraction of crystalline phase declined drastically in the presence of alumina especially in 40 wt%. Therefore, the addition of large amounts of alumina should be avoided if the

purpose is to achieve high crystalline HAp–composite nanopowder. It should be noted that the subsequent annealing can be used to crystallize the composite nanopowders, but the interfacial reaction may happen during the annealing. This phenomenon leads to the formation of additional phases which has adverse effects on the biological responses and mechanical properties of the HAp-based composites.

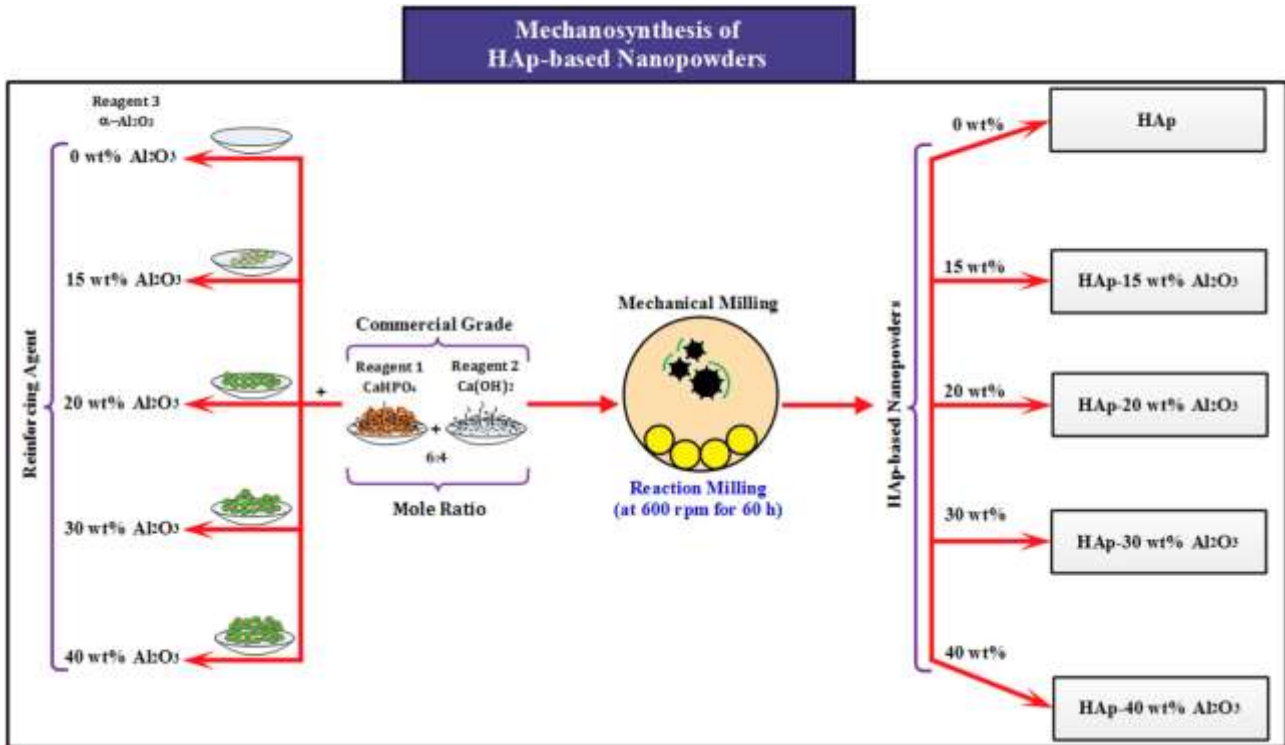


Fig. 9 The reaction mechanism of the formation of HAp–Al₂O₃ composite nanopowders during the mechanochemical synthesis.

4. Conclusions

To sum up, the preparation of HAp–Al₂O₃ composite nanopowders by the mechanochemical process was studied. The results of this work can be summarized as follows:

1. The mechanochemical behaviour of the $\text{CaHPO}_4\text{--Ca(OH)}_2\text{--Al}_2\text{O}_3$ system was strongly influenced by the alumina content. In the absence of alumina, the main product of milling for 60 h was HAp nanopowder with the crystallite size of about 24 nm. From TEM image, the HAp nanopowder showed high tendency to agglomerate due to the coalescence of fine particles. However, each agglomerate was composed of nanorods with a mean size of about 17 ± 8 nm.
2. With the addition of various amounts of alumina, mechanical activation for 60 h resulted in the formation of HAp–Al₂O₃ composite nanopowders with the crystallite size of about 34, 28, 27, and 24 nm in the presence of 15, 20, 30, and 40 wt% alumina, respectively. However, additional peaks belonging to CaHPO_4 was detected in all the samples.
3. The results suggest that the crystallinity degree of the mechanothesized HAp bioceramics was effectively influenced by the alumina content. The crystallinity degree was around 83 % in the absence of reinforcing agent, while this value declined drastically to about 16 % in the presence of 40 wt% alumina.
4. In accordance with the proposed reaction mechanism, no interfacial reaction occurred between the calcium phosphate reagents and alumina. In a nutshell, the proposed reaction provides a facile way to obtain HAp–Al₂O₃ composite nanopowders with appropriate structural features.

Acknowledgment

The authors are grateful to research affairs of Islamic Azad University, Najafabad Branch for supporting of this research.

References

- Ben-Nissan B. (2004). Nanoceramics in Biomedical Applications, *MRS Bulletin* 29, 28-32.
- Best S.M., Porter A.E., Thian E.S., Huang J. (2008). Bioceramics: Past, present and for the future, *J. Eur. Ceram. Soc.* 28, 1319-1327.
- Chen Y., Miao X. (2005). Thermal and chemical stability of fluorohydroxyapatite ceramics with different fluorine contents, *Biomaterials* 26, 1205-1210.
- Ebrahimi-Kahrizsangi R., Nasiri-Tabrizi B., Chami A. (2010). Synthesis and characterization of fluorapatite–titania (FAP–TiO₂) nanocomposite via mechanochemical process, *Solid State Sci.* 12, 1645-1651.
- Ebrahimi-Kahrizsangi R., Nasiri-Tabrizi B., Chami A. (2011). Characterization of single-crystal fluorapatite nanoparticles synthesized via mechanochemical method, *Particuology* 9, 537-544
- Fahami A., Nasiri-Tabrizi B., Ebrahimi-Kahrizsangi R. (2013). Mechanochemical synthesis and characterization of chlorapatite nanopowders, *Mater. Lett.* 110, 117-121.
- Fathi M.H., Mohammadi Zahrani E. (2009). Mechanical alloying synthesis and bioactivity evaluation of nanocrystalline fluoridated hydroxyapatite, *J. Cryst. Growth* 311, 1392-1403.
- Hench L.L. (1998). Bioceramics. *J. Amer. Ceram. Soc.* 81, 1705-1728.
- Honarmandi P., Honarmandi P., Shokuhfar A., Nasiri-Tabrizi B., Ebrahimi-Kahrizsangi R. (2010). Milling media effects on synthesis, morphology and structural characteristics of single crystal hydroxyapatite nanoparticles, *Adv. Appl. Ceram.* 109, 117-122.
- Kim S., Kong Y.M., Lee I.S., Kim H.E. (2002). Effect of calcinations of starting powder on mechanical properties of hydroxyapatite–alumina bioceramic composite, *J. Mater. Sci.: Mater. Med.* 13, 307-310.
- Kong Y.M., Kim S., Kim H.E. (1999). Reinforcement of hydroxyapatite bioceramic by addition of ZrO₂ coated with Al₂O₃, *J. Amer. Ceram. Soc.* 82, 2963-2968.
- Kuntz J. D., Zhan G.D., Mukherjee A.K. (2004). Nanocrystalline-Matrix Ceramic Composites for Improved Fracture Toughness, *MRS Bulletin* 29, 22-27.
- Li B., Guo B., Fan H., Zhang X. (2008). Preparation of nano-hydroxyapatite particles with different morphology and their response to highly malignant melanoma cells in vitro, *Appl. Surf. Sci.* 255, 357-360.
- Li J., Fartash B., Hermansson L. (1995). Hydroxyapatite-alumina composites and bone-bonding, *Biomaterials* 16, 417-422.
- Nasiri-Tabrizi B., Honarmandi P., Ebrahimi-Kahrizsangi R., Honarmandi P. (2009). Synthesis of nanosize single-crystal hydroxyapatite via mechanochemical method, *Mater. Lett.* 63, 543-546.
- Nasiri-Tabrizi B., Fahami A., Ebrahimi-Kahrizsangi R. (2013a). Effect of milling parameters on the formation of nanocrystalline hydroxyapatite using different raw materials, *Ceram. Int.* 39, 5751-5763.
- Nasiri-Tabrizi B., Fahami A. (2013b) Effect of zirconia content on the mechanochemical synthesis and structural features of fluorapatite-based composite nanopowders, *Ceram. Int.* 39, 7331-7342.
- Nasiri-Tabrizi B., Fahami A., Ebrahimi-Kahrizsangi R. (2014). Phase transitions and structural changes of nanostructured chlorapatite under thermal treatment, *Ceram. Int.* 40, 901-910
- Pushpakanth S., Srinivasan B., Sreedhar B., Sastry T.P. (2008). An in situ approach to prepare nanorods of titania hydroxyapatite (TiO₂–HAp) nanocomposite by microwave hydrothermal technique, *Mater. Chem. Phys.* 107, 492-498.
- Sanosh K.P., Chu M.C., Balakrishnan A., Lee Y.J., Kim T.N., Cho S.J. (2009). Synthesis of nano hydroxyapatite powder that simulate teeth particle morphology and composition, *Curr. Appl. Phys.* 9, 1459-1462.
- Seckler M.M., Danese M., Derenzo S., Valarelli J.V., Giulietti M., Rodriguez-Clemente R. (1999). Influence of process conditions on hydroxyapatite crystallinity obtained by direct crystallization, *J. Mater. Res.* 2, 59-62.
- Silva C.C., Valente M.A., Graça M.P.F., Sombra A.S.B. (2004). Preparation and optical characterization of hydroxyapatite and ceramic systems with titanium and zirconium formed by dry high-energy mechanical alloying, *Solid State Sci.* 6, 1365-1374.
- Sun F., Froes F.H.S. (2002). Synthesis and characterization of mechanical alloyed Ti_xMg alloys, *J. Alloy. Compd.* 340, 220-225.
- Suryanarayana C. (2001). Mechanical alloying and milling, *Prog. Mater. Sci.* 46, 1-184.

- Viswanath B., Ravishankar N. (2006). Interfacial reactions in hydroxyapatite/alumina nanocomposites, *Scripta Mater.* 55, 863-866.
- Zhang J., Lin Zh., Lan Y., Ren G., Chen D., Huang F., Hong M. (2006). A multistep oriented attachment kinetics: coarsening of ZnS nanoparticle in concentrated NaOH, *J. Amer. Chem. Soc.* 128, 12981-12987.
- Zhou H., Lee J. (2011). Nanoscale hydroxyapatite particles for bone tissue engineering, *Acta Biomaterialia* 7, 2769-2781.